Constant-Frequency Constrained Optimal Direct Power Control of Voltage-Source PWM Rectifiers

Nimród KUTASI, Katalin GYÖRGY and András KELEMEN

Abstract *- The PWM voltage source rectifier analyzed in this paper exhibits both continuous and discrete dynamic behavior and therefore represents a hybrid dynamic system. The jump condition between switching states is defined by the control space vector. Direct Power Control (DPC) is a control method tailored to such hybrid systems, and its optimization has been considered by several authors. However, the constraints are usually disregarded, leading to unrealistic results. The paper presents the constant frequency Model Predictive Direct Power Control (MP-DPC) of the PWM voltage source rectifier using two types of symmetrical switching patterns. The control algorithms are validated by Matlab Simulink modeling and simulation.*

Keywords*: direct power control, predictive model, voltage source, PWM rectifier.*

1. INTRODUCTION

In case of a voltage-sourse PWM rectifier the task is to control the DC-side voltage, while ensuring unity power factor at the line side [2],[3],[4],[5],[6]. Thus, the rectified voltage has to be regulated to a voltage level required by the load, which is higher than the peak value of the mains line voltage (boost-type rectifier). This level of the DC voltage makes possible the control of the line currents by means of the rectifier input voltage system synthesized in a proper way. In case of a symmetrical, sinusoidal supply voltage system, the line currents are controlled to be sinusoidal and in phase with the mains voltage system.

A solution of this problem is based on the instantaneous power theory [1]. According to this theory, the above targets can be reached if the instantaneous real power is regulated to the value prescribed by the DC voltage controller and the instantaneous imaginary power is regulated to zero.

The paper presents an online approach to the PWM rectifier control, based on the instantaneous power theory. In order to synthesize the rectifier input voltage that tends to fulfill the above targets, the solution employs the rectifier input voltage vectors neighboring with the actual line voltage vector.

A specific form of space vector modulation (SVM) is used to synthesize the rectifier input voltage vector. According to this SV modulation method presented in [2], the lengths of the subintervals of the switching period are determined in order to minimize a cost function. Each subinterval corresponds to a switch configuration i.e. to a control space vector. Thus, the Direct Power Control (DPC) algorithm used to control the instantaneous real and imaginary powers, supplies directly the length of the time intervals instead of the components of the control vector.

Manuscript received April 30, 2010. This work has been supported by the Institute for Research Programmes of the Sapientia University.

2. CONSTANT-FREQUENCY CONSTRAINED OPTIMAL CONTROL

The model of the PWM rectifier is derived based on the space vector theory. The space vectors are defined in a way that makes possible the simplest calculation of the instantaneous power from the two-phase voltage and current components. Thus

$$\underline{u} = u_\alpha + ju_\beta = \sqrt{\frac{2}{3}}\left(u_a + \underline{a}u_b + \underline{a}^2 u_c\right) \quad \text{and} \qquad (1)$$

$$\underline{i} = i_\alpha + ji_\beta = \sqrt{\frac{2}{3}}\left(i_a + \underline{a}i_b + \underline{a}^2 i_c\right) \qquad (2)$$

are the space vectors of the mains supply phase voltages and line currents. In a similar manner the space vector of the rectifier input voltage results as

$$\underline{u}_R = u_{R\alpha} + ju_{R\beta} = \sqrt{\frac{2}{3}}\left(u_{Ra} + \underline{a}u_{Rb} + \underline{a}^2 u_{Rc}\right), \qquad (3)$$

and it is defined by the DC voltage u_d and by the switching states of the transistors from the rectifier bridge. Due to the fact that the devices from a rectifier leg are controlled complementarily, the switching states of the six devices can be described by the space vector

$$\underline{\delta} = \delta_\alpha + j\delta_\beta = \delta_a + \underline{a}\delta_b + \underline{a}^2\delta_c\,, \qquad (4)$$

where $\delta_i = 1$ if the upper transistor is ON and $\delta_i = 0$ if the lower transistor is ON.

Using the matrix formulation,

© 2010 – Mediamira Science Publisher. All rights reserved.

$$[i]^T=[i_a\ i_b\ i_c],\quad [\delta]^T=[\delta_a\ \delta_b\ \delta_c]. \tag{5}$$

The rectifier output current (Fig.1) can be calculated as the sum of the currents flowing through the high-side devices (6)

$$i_o=[i]^T[\delta]\ , \tag{6}$$

and can be expressed using the two-phase components of the space vectors as follows.

$$[i]_\perp=\begin{bmatrix} i_\alpha \\ i_\beta \\ i_h \end{bmatrix}=\sqrt{\frac{3}{2}}[A][i],[\delta]_\perp=\begin{bmatrix} \delta_\alpha \\ \delta_\beta \\ \delta_h \end{bmatrix}=\sqrt{\frac{3}{2}}[A][\delta], \tag{7}$$

where

$$[A]=\frac{2}{3}\begin{bmatrix} 1 & -\frac{1}{2} & -\frac{1}{2} \\ 0 & \frac{\sqrt{3}}{2} & -\frac{\sqrt{3}}{2} \\ \frac{1}{2} & \frac{1}{2} & \frac{1}{2} \end{bmatrix}. \tag{8}$$

From (7) it results:

$$[i]=\sqrt{\frac{2}{3}}[A]^{-1}[i]_\perp,\quad [\delta]=\sqrt{\frac{2}{3}}[A]^{-1}[\delta]_\perp \tag{9}$$

where

$$[A]^{-1}=\begin{bmatrix} 1 & 0 & 1 \\ -\frac{1}{2} & \frac{\sqrt{3}}{2} & 1 \\ -\frac{1}{2} & -\frac{\sqrt{3}}{2} & 1 \end{bmatrix}. \tag{10}$$

Thus

$$i_o=[i]^T[\delta]=\frac{2}{3}\left([A]^{-1}[i]_\perp\right)^T\left([A]^{-1}[\delta]_\perp\right)=$$

$$=\frac{2}{3}[i]_\perp^T\begin{bmatrix} \frac{3}{2} & 0 & 0 \\ 0 & \frac{3}{2} & 0 \\ 0 & 0 & 3 \end{bmatrix}[\delta]_\perp=\begin{bmatrix} i_\alpha & i_\beta & 2i_h \end{bmatrix}\begin{bmatrix} \delta_\alpha \\ \delta_\beta \\ \delta_0 \end{bmatrix}= \tag{11}$$

$$=\left[i_\alpha\delta_\alpha+i_\beta\delta_\beta\right]=\mathrm{Re}\left(\underline{i}\underline{\delta}^*\right)$$

because the i_h zero-sequence component of the line current system is zero (12).

$$i_h=\frac{1}{3}\left(i_a+i_b+i_c\right). \tag{12}$$

The voltage equation for the phase *i* can be written as:

$$u_i=L\frac{d}{dt}i_i+Ri_i+u_{iN}+u_{N0} \tag{13}$$

The voltage term u_{N0} disappears from the vectorial voltage equation because it's a zero-sequence component. Taking into account (11), the mathematical model of the rectifier in the two-phase stationary reference frame is given by the equations:

$$\begin{aligned} u_{\alpha\beta}&=L\frac{d}{dt}i_{\alpha\beta}+Ri_{\alpha\beta}+u_{R\alpha\beta} \\ C_d\frac{d}{dt}u_d&=\mathrm{Re}\left(\underline{i}\underline{\delta}^*\right)-i_T \\ u_{R\alpha\beta}&=\sqrt{\frac{2}{3}}u_d\delta_{\alpha\beta} \end{aligned}\ . \tag{14}$$

The instantaneous power at the rectifier input is defined by:

$$\begin{aligned} \underline{s}&=p+jq=\underline{u}\underline{i}^*=\left(u_\alpha+ju_\beta\right)\left(i_\alpha-ji_\beta\right)= \\ &=\left(u_\alpha i_\alpha+u_\beta i_\beta\right)+j\left(u_\beta i_\alpha-u_\alpha i_\beta\right) \end{aligned} \tag{15}$$

Let us consider a cost function (16) defined using the instantaneous real and imaginary power errors at the end of the next switching cycle.

$$J=\left(p_{ref}-p_{t_0+T_s}\right)^2+\left(q_{ref}-q_{t_0+T_s}\right)^2 \tag{16}$$

The value of this cost function can be estimated by linearization of the instantaneous powers' time function around the actual time instant. Time derivative of the instantaneous power is calculated based on the converter model and on the measurement results from the beginning of the next in turn switching cycle.

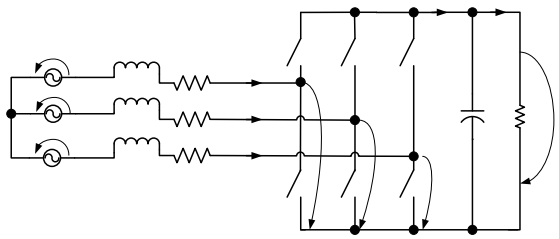

Fig. 1. Simplified circuit diagram of the voltage source PWM rectifier.

Thus, the estimated powers at $t=t_0+\Delta t$ are:

$$\begin{aligned} p_{t_0+\Delta t}&=p_{t_0}+h_p\Delta t \\ q_{t_0+\Delta t}&=q_{t_0}+h_q\Delta t \end{aligned}\ , \tag{17}$$

where

$$h_p=\frac{dp}{dt}\Big|_{t=t_0},\quad h_q=\frac{dq}{dt}\Big|_{t=t_0}$$

are the time derivatives at the beginning of the switching cycle. Using the definition of the instantaneous powers, it results:

$$\begin{aligned} h_p&=\left(u_\alpha\frac{di_\alpha}{dt}+i_\alpha\frac{du_\alpha}{dt}+u_\beta\frac{di_\beta}{dt}+i_\beta\frac{du_\beta}{dt}\right)\Big|_{t=t_0} \\ h_q&=\left(u_\beta\frac{di_\alpha}{dt}+i_\alpha\frac{du_\beta}{dt}-u_\alpha\frac{di_\beta}{dt}-i_\beta\frac{du_\alpha}{dt}\right)\Big|_{t=t_0} \end{aligned}\ . \tag{18}$$

For simple notation all quantities will be considered at $t=t_0$ unless otherwise specified.

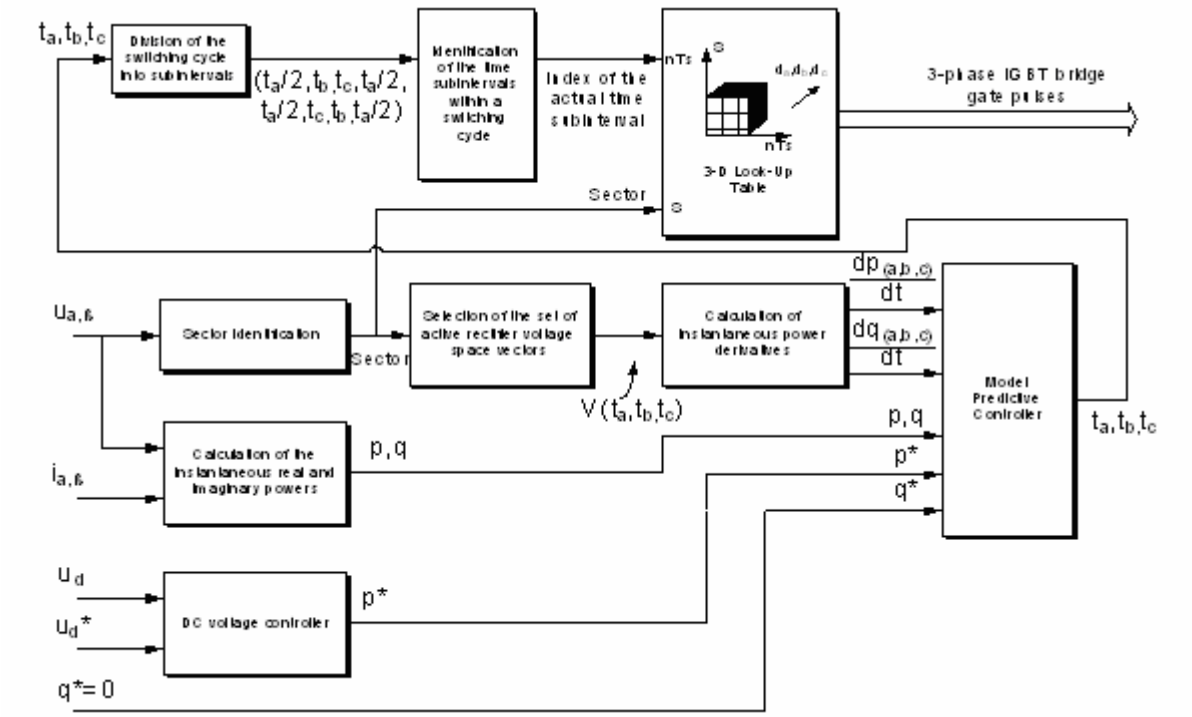

Fig. 2. Block structure of the MP-DPC controller.

From the voltage equation the derivatives of the current components can be expressed as:

$$\frac{di_{\alpha\beta}}{dt} = \frac{1}{L}\left(u_{\alpha\beta} - u_{R\alpha\beta} - Ri_{\alpha\beta}\right). \tag{19}$$

The time derivative of the symmetrical and sinusoidal three-phase supply voltage is:

$$\frac{d\underline{u}}{dt} = j\omega\underline{u}. \tag{20}$$

Thus, the components of the supply voltage vector derivative are:

$$\begin{aligned} \mathrm{Re}\left(\frac{d\underline{u}}{dt}\right) &= -\omega u_\beta \\ \mathrm{Im}\left(\frac{d\underline{u}}{dt}\right) &= \omega u_\alpha \end{aligned} \tag{21}$$

The derivatives of the instantaneous powers result as:

$$\begin{aligned} \frac{dp}{dt} &= u_\alpha\left(\frac{1}{L}\left(u_\alpha - u_{R\alpha} - Ri_\alpha\right) + \omega i_\beta\right) + \\ &+ u_\beta\left(\frac{1}{L}\left(u_\beta - u_{R\beta} - Ri_\beta\right) - \omega i_\alpha\right) \\ \frac{dq}{dt} &= u_\alpha\left(-\frac{1}{L}\left(u_\beta - u_{R\beta} - Ri_\beta\right) + \omega i_\alpha\right) + \\ &+ u_\beta\left(\frac{1}{L}\left(u_\alpha - u_{R\alpha} - Ri_\alpha\right) + \omega i_\beta\right) \end{aligned} \tag{22}$$

The block structure of the MP-DPC controller is shown in Fig.2. The instantaneous imaginary power reference is set to zero, while the reference of the instantaneous real power is given by the output of the DC voltage controller.

An optimal control is obtained by choosing the control vector which minimizes the cost function (16).

In Fig.3 the supply voltage vector from an arbitrarily chosen moment is shown in the complex plane along with the rectifier input voltage vectors corresponding to the possible switching states of the rectifier. The rectifier input vectors divide the complex plane into 6 sectors and these vectors are obtained from the DC voltage and the control vectors according to (14).

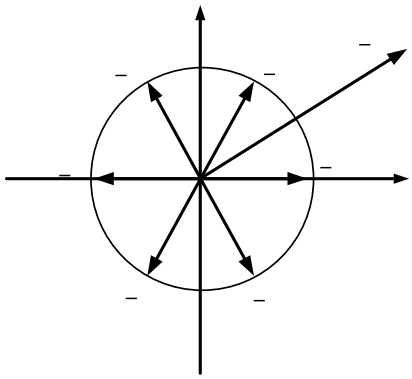

Fig. 3. Rectifier input voltage vectors and the line voltage vector in the first sector of the complex plane.

According to the constant frequency control approach described in [2], the optimal control vector is synthesized from the control vectors delimiting the sector which contains the input voltage vector, and the complex plane is divided into 12 sectors. This solution is adopted in order to minimize the line current ripple.

Fig.4 shows the variation in time of the power derivatives that could be produced by the application of the $\underline{u}_{R1}$ rectifier input voltage vector. The constant-frequency DPC method applies this vector only in the first and second sectors.

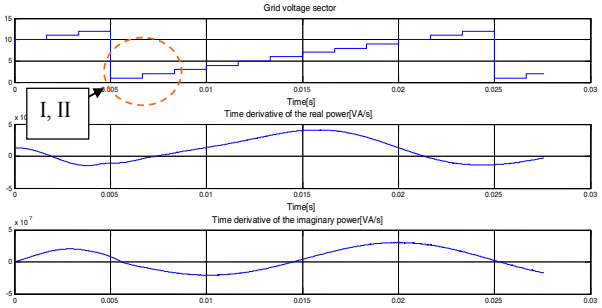

Fig. 4. Variation of the real and imaginary power derivatives corresponding to the $\underline{u}_{R1}$ rectifier input voltage vector.

Fig.4 illustrates the possibility to influence the evolution of the real and imaginary powers in different time intervals defined by the position of the grid voltage vector. Three voltage vectors are employed in each time interval. It can be observed that with only 4 milliseconds after start-up, the derivatives can be made both positive and negative, as required by the Direct Power Control.

Fig.5 demonstrates that the instantaneous powers become controllable when the DC voltage becomes higher than the level imposed by the boost operation, which is a natural result.

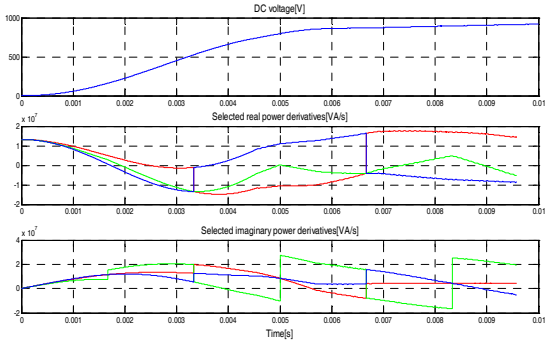

Fig. 5. Relationship between the DC voltage level and the controllability of the instantaneous powers. Both signs of the derivatives are guaranteed for Ud>560V.

According to the symmetrical switching pattern proposed by this paper, the switching period is divided into 8 time intervals (ta/2, tb, tc, ta/2, ta/2, tc, tb, ta/2). Thus, in a similar way to [2], where the division is (ta, tb, tc, tc, tb, ta), the lengths of 3 time intervals have to be chosen in order to optimize the cost function on a horizon of one switching period, i.e. 8 switching states.

Assuming that the variation during a switching period of the supply voltage, supply current and DC voltage are negligible, the time derivatives of the instantaneous powers in the 8 time intervals can be calculated from (22) based only on the measurement results from the beginning of that switching period.

In a similar manner to (16), the cost function at the end of the switching period can be estimated as:

$$J = \left(p_{ref} - p - 2h_{pa}t_a - 2h_{pb}t_b - 2h_{pc}t_c\right)^2 + \left(q_{ref} - q - 2h_{qa}t_a - 2h_{qb}t_b - 2h_{qc}t_c\right)^2 =$$
$$= \left(p_{ref} - p - h_{pc}T_s + 2t_a\left(h_{pc} - h_{pa}\right) + 2t_b\left(h_{pc} - h_{pb}\right)\right)^2 +$$
$$+ \left(q_{ref} - q - h_{qc}T_s + 2t_a\left(h_{qc} - h_{qa}\right) + 2t_b\left(h_{qc} - h_{qb}\right)\right)^2 \tag{23}$$

Determination of the optimal t_a, t_b, t_c is equivalent to solving a quadratic programming problem with constraints shown in Fig.6, i.e.

$$0 \le t_a,\ 0 \le t_b,\ t_a + t_b \le \frac{T_s}{2}\ . \tag{24}$$

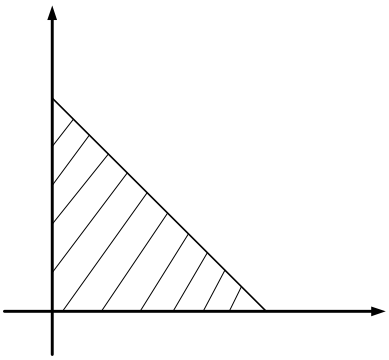

Fig. 6. The limits of the switching time intervals..

The problem is solved reducing the inequality-type constraints to equality-type constraints corresponding to the edges and vertices of the convex polygon defined by (24). For instance, the constrained minimum with the constraint $t_a = 0$ results by minimization of the cost function (25).

$$J = \left(p_{ref} - p - 2\left(h_{pb}t_b + h_{pc}\left(\frac{1}{2}T_s - t_b\right)\right)\right)^2 +$$
$$+ \left(q_{ref} - q - 2\left(h_{qb}t_b + h_{qc}\left(\frac{1}{2}T_s - t_b\right)\right)\right)^2 \tag{25}$$

If the minimum of (25) belongs to the (OA) segment, it is considered a valid candidate for optimal solution. Otherwise one of the vertices (O) and (A) minimize (25).

With $p_{err} = p - p_{ref}$ and $q_{err} = q - q_{ref}$, the constrained optimum is given by one of the following triplets:

1.)
$$t_a = \frac{-p_{err}\left(h_{qb} - h_{qc}\right) - q_{err}\left(h_{pc} - h_{pb}\right) + T_s\left(h_{pb}h_{qc} - h_{pc}h_{qb}\right)}{2\left(h_{pa}\left(h_{qb} - h_{qc}\right) + h_{pb}\left(h_{qc} - h_{qa}\right) + h_{pc}\left(h_{qa} - h_{qb}\right)\right)}$$
$$t_b = \frac{-p_{err}\left(h_{qc} - h_{qa}\right) - q_{err}\left(h_{pa} - h_{pc}\right) + T_s\left(h_{pc}h_{qa} - h_{pa}h_{qc}\right)}{2\left(h_{pa}\left(h_{qb} - h_{qc}\right) + h_{pb}\left(h_{qc} - h_{qa}\right) + h_{pc}\left(h_{qa} - h_{qb}\right)\right)}\ ; \tag{26}$$
$$t_c = \frac{T_s}{2} - t_a - t_b$$

which represents the unconstrained minimum, also presented in [2].

$$2.)\ \begin{cases} t_a = \dfrac{T_s}{2} \\ t_b = 0 \\ t_c = 0 \end{cases} ; \qquad (27)$$

$$3.)\ \begin{cases} t_a = \dfrac{-p_{err}\left(h_{pa}-h_{pc}\right)-q_{err}\left(h_{qa}-h_{qc}\right)+T_s\left(h_{pc}\left(-h_{p1}+h_{p3}\right)+h_{qc}\left(-h_{q1}+h_{q3}\right)\right)}{2\left(\left(h_{pa}-h_{pc}\right)^2+\left(h_{qa}-h_{qc}\right)^2\right)} \\ t_b = 0 \\ t_c = \dfrac{T_s}{2}-t_a \end{cases} \qquad (28)$$

$$4.)\ \begin{cases} t_a = 0 \\ t_b = \dfrac{-p_{err}\left(h_{pb}-h_{pc}\right)-q_{err}\left(h_{qb}-h_{qc}\right)+T_s\left(h_{pc}\left(-h_{pb}+h_{pc}\right)+h_{qc}\left(-h_{qb}+h_{qc}\right)\right)}{2\left(\left(h_{pb}-h_{pc}\right)^2+\left(h_{qb}-h_{qc}\right)^2\right)} \\ t_c = \dfrac{T_s}{2}-t_b \end{cases} \qquad (29)$$

$$5.)\ \begin{cases} t_a = 0 \\ t_b = \dfrac{T_s}{2} \\ t_c = 0 \end{cases} \qquad (30)$$

$$6.)\ \begin{cases} t_a = 0 \\ t_b = 0 \\ t_c = \dfrac{T_s}{2} \end{cases} \qquad (31)$$

$$7.)\ \begin{cases} t_a = \dfrac{-p_{err}\left(h_{pa}-h_{pb}\right)-q_{err}\left(h_{qa}-h_{qb}\right)+T_s\left(\left(-h_{pb}+h_{pc}\right)\left(h_{pa}-h_{pb}\right)+\left(-h_{qb}+h_{qc}\right)\left(h_{qa}-h_{qb}\right)\right)}{2\left(\left(h_{pa}-h_{pb}\right)^2+\left(h_{qa}-h_{qb}\right)^2\right)} \\ t_b = \dfrac{T_s}{2}-t_a \\ t_c = 0 \end{cases} \qquad (32)$$

Expressions (27), (30), (31) and (28), (29), (32) represent the vertices and the edges of the polygon from Fig.6.

Using the switching pattern from [2] built for a division of the complex plane into 12 sectors, variation of the line currents during the converter start-up is shown in Fig.7, while Fig.8 presents the evolution of the real and imaginary power errors.

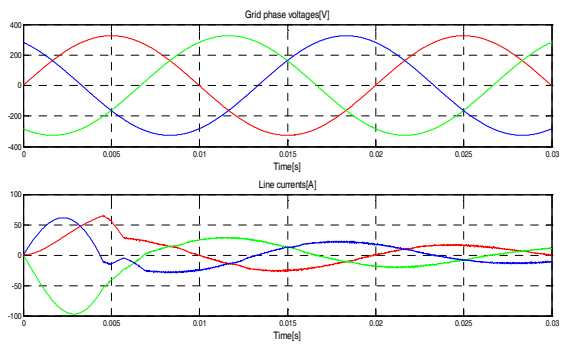

Fig. 7. Start-up of the rectifier in case of constant-frequency constrained optimal DPC control.

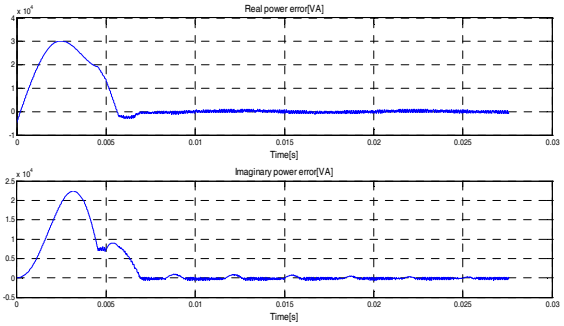

Fig. 8. Evolution of the real and imaginary power errors during te start-up process. It can be noticed that steady-state values are reached in 6-7 ms.

A symmetrical switching pattern can be defined also for a division of the complex plane into only 6 sectors. In Fig.10 the states of the upper switches are shown for each sector under the assumption of $t_a = t_b = t_c$, chosen for simplification of the drawing.

The trajectory of the switching states in the fifth sector is shown in Fig.9. It can be observed that the switching pattern is built in a way that only a single power transistor is switched at once (meaning a transition between two adjacent vertices of the cube from Fig.9). The transition between two adjacent sectors is made also by switching a single transistor.

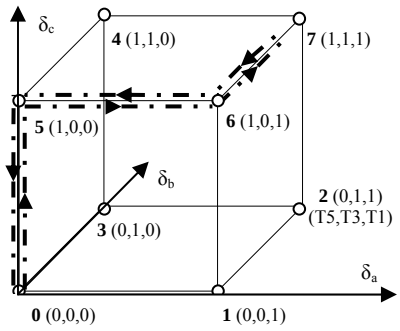

Fig. 9. The trajectory of the control vector obtained by application of the switching pattern from Fig.10 in the fifth sector.

Fig.11 and Fig.12 make possible the comparison of the space trajectories obtained using the pulse patterns presented in [2] (Fig.12), respectively using the pulse patterns proposed in this paper (Fig.11) in case of start-up of the rectifier in identical conditions. A smaller ripple of the control space vector can be observed in case of the switching patterns shown in Fig.11.

3. CONCLUSIONS

Constant switching frequency constrained optimal online control of a three-phase voltage-source rectifier has been presented. The cost function is based on the instantaneous power errors. The imposed constraints are represented by the limits of the time intervals available for of different switch configurations.

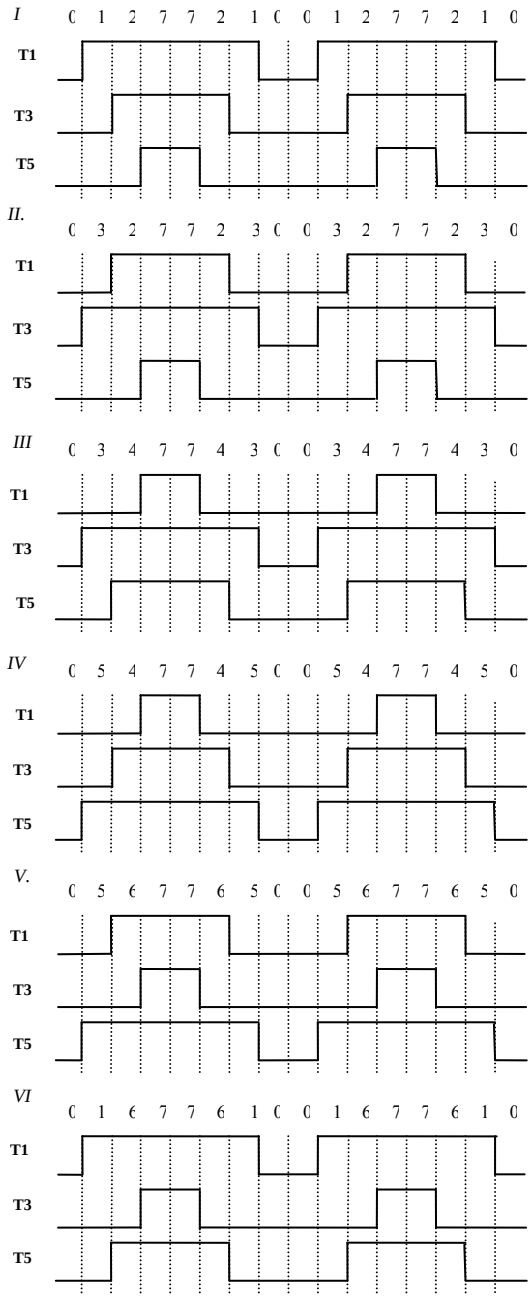

Fig. 10. Switching pattern defined for 6 sectors.

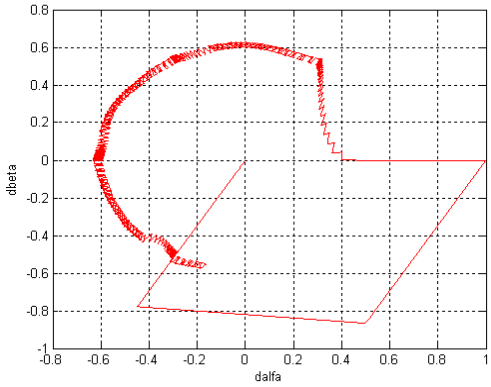

Fig. 11. Trajectory of the control vector in case of 6 sectors of the complex plane and 8 subintervals of the switching cycle.

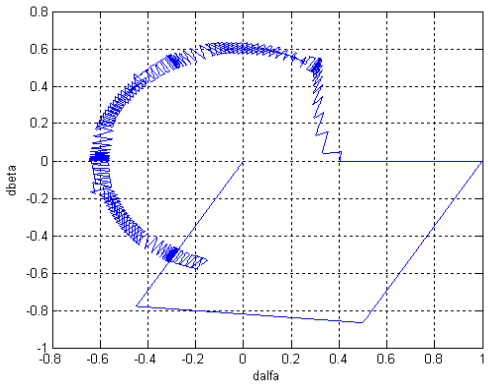

Fig. 12. Trajectory of the control vector in case of 12 sectors of the complex plane and 6 subintervals of the switching cycle.

A symmetrical switching pattern has been implemented, which applies both $\underline{u}_{R0}$ and $\underline{u}_{R7}$ in each switching cycle divided into 8 subintervals. The ripple of the control vector is reduced due to the increased number of switch transitions in a switching cycle and due to the improved pattern.

The operation with Constant Frequency Model Predictive Control has been analyzed by Matlab Simulink modeling and simulation.

REFERENCES

1. H. Akagi, E.H. Watanabe, M. Aredes, "Instantaneous Power Theory and Applications to Power Conditioning", *Wiley-Interscience*, 2007.
2. P. Antoniewicz, "Predictive Control of Three Phase AC/DC Converters, Phd Thesis", *Warsaw University of Technology*, 2009.
3. M. Malinowski, M. Jasinski, and M.P. Kazmierkowski, "Simple Direct Power Control of Three-Phase PWM Rectifier Using Space-Vector Modulation (DPC-SVM)", *IEEE Transactions on Industrial Electronics*, Vol. 51, No. 2, pp. 447-454, 2004.
4. S. Vazquez, J.A. Sanchez, J.M. Carrasco, J.I. Leon, E. Galvan, "A Model-Based Direct Power Control for Three-Phase Power Converters", *IEEE Transactions on Industrial Electronics*, Vol. 55, No. 4, pp. 1647-1657, Apr. 2008.
5. J.M. Carrasco, E. Galvan, G. Escobar, A.M. Stankovic', R. Ortega, "Direct active and reactive power control (DPQ) for a three phase synchronous rectifier", in *Proceedings of the 31st Power Electronics Specialists Conference PESC00*, Vol. 2, pp. 737-742, 2000.
6. G. Escobar, A.M. Stankovic'. J.M. Carrasco, E. Galván, and R. Ortega, "Analysis and design of direct power control (DPC) for a three phase synchronous rectifier via output regulation subspaces", *IEEE Transactions on Power Electronics*, Vol. 18, No. 3, pp. 823-830, May 2003.

Nimród KUTASI
Katalin GYÖRGY
András KELEMEN

Sapientia University
Department of Electrical Engineering
Tîrgu Mureş, Romania
E-mail: kutasi@ms.sapientia.ro, kgyorgy@ms.sapientia.ro, kandras@ms.sapientia.ro